

INVESTIGATION OF MULTILAYER MAGIC-T CONFIGURATIONS USING NOVEL MICROSTRIP-SLOTLINE TRANSITIONS

W. Marynowski* and J. Mazur

Faculty of Electronics, Telecommunications and Informatics, Gdansk University of Technology, Gdansk, Poland

Abstract—Two novel compact magic-T configurations designed as a two layer structure are proposed in this paper. They consist of a microstrip tee-junction and resonance circuit composed of a microstrip line combined with rectangular or radial stubs. These microstrip circuits are respectively printed at the top and bottom layers of the structure, and coupled via a slot located in the common ground plane. The microstrip patch and slot are placed parallel to each other forming novel microstrip-slotline transitions, which provide broadband operation of the magic-Ts. Transmission line equivalent circuits are used to explain the performance of the proposed hybrids. It is shown that magic-T with a radial stub demonstrates wider operation bandwidth and better performance than the structure with a rectangular stub. In order to validate their performance, the prototypes of both configurations were manufactured and measured. Experimental and simulation results show that the resulting magic-T using a radial resonator has a fractional bandwidth of over 40% for 0.2 dB amplitude and 0.5° phase imbalance. The experimental results are in good agreement well with equivalent circuit and full-wave simulations.

1. INTRODUCTION

Recently, integrated magic-T structures have been widely used at microwave/millimetre wave frequencies as functional components of complex microwave circuits and systems. They belong to a wider group of passive components that allow for signal division [1–25]. The magic-Ts are four-port devices that offer in-phase and out-of-phase signal division between their two output ports [11–25].

Received 23 March 2012, Accepted 24 May 2012, Scheduled 13 June 2012

* Corresponding author: Wojciech Marynowski (wojmar@eti.pg.gda.pl).

They are constructed with many different integrated planar circuits such as branch-line, rat-race or directional couplers [11]. In order to improve their performances, double-sided and two-layer magic-T components have been proposed in [12–25]. These configurations using coplanar [12], microstrip [13–21] or substrate integrated waveguide (SIW) [22–25] to slotline field conversion broaden the bandwidth of magic-Ts. Such configurations are mostly composed of a microstrip-slotline transition and a tee-junction circuit. The tee-junction ports represent sum and dividing ports of the magic-T, while the port of the transition forms the difference one. Several double-sided structures consist of the tee-microstrip and slotline circuits oppositely located on the common substrate and coupled through microstrip-slotline transitions [12–16]. These structures are characterized by 40% up to 50% fractional bandwidth with isolation between the sum and difference ports better than 40 dB. However, there is large radiation from the slotline structure, which causes higher insertion losses in these networks.

Reduction of the losses appears in the configurations with small slot apertures as reported in [17–20]. These devices, as well as double-sided configurations, are designed on a single substrate. The slotline is formed in a ground plane and the microstrip circuits of the tee-junction and transition are printed on the same side of the substrate. This construction has microstrip ports in the same plane offering easy integration with other microstrip circuits located on the same substrate.

Another compact magic-T is designed as a two layer structure. The microstrip tee-junction and microstrip-slotline transition are performed on the separate substrates and coupled via a slot located in the common ground plane. In several magic-T constructions the SIW waveguide [22–25] is implemented in the transition instead of the microstrip. To obtain proper coupling conditions, the slot can be cut transversely or longitudinally in the ground of the SIW guide. Its position in the microstrip line is perpendicular to the strip, as in the conventional microstrip to slotline transition [26, 27]. However, in this design parallel ports of the transition and tee-junction are located on the opposite layers [21], which may limit the use of such a design in highly integrated microwave systems. In addition, application of the electrically short slot resonator causes a narrow operating bandwidth which is less than 25%. Due to the compact construction of mentioned devices, the isolation between sum and difference ports is less than 30 dB. Since the field in the slotline is enclosed by the microstrip circuits of the tee-junction and transition, the slot radiation is reduced which, ipso facto, decreases the insertion losses of these magic-T

arrangements.

In this paper, two novel microstrip-slotline transitions based on the broadside coupling between parallel microstrip patch and slot are adopted to design two-layer magic-T configurations. The theoretical basis and design procedure of the proposed configurations are based upon the general integrated magic-T principles, and their performance has been verified numerically using full wave commercial software. The operation principles and design of the magic-T arrangements are described in Section 2. In Section 3 the magic-Ts' simulated scattering frequency characteristics are illustrated and verified by results obtained from measurements of their prototypes.

2. DESIGN CONCEPT AND EQUIVALENT MODEL

2.1. Configurations of the Proposed Magic-Ts

The circuit layouts of both magic-Ts are shown in Fig. 1. Their structures consist of three metalized planes separated by two dielectric substrates. On the top layer the microstrip patch is printed. A microstrip tee-junction configuration is positioned on the bottom layer. The central plane represents a common ground where a coupling slot-aperture is etched. The considered configurations are similar to the one reported in [21] where the conventional transition with microstrip and

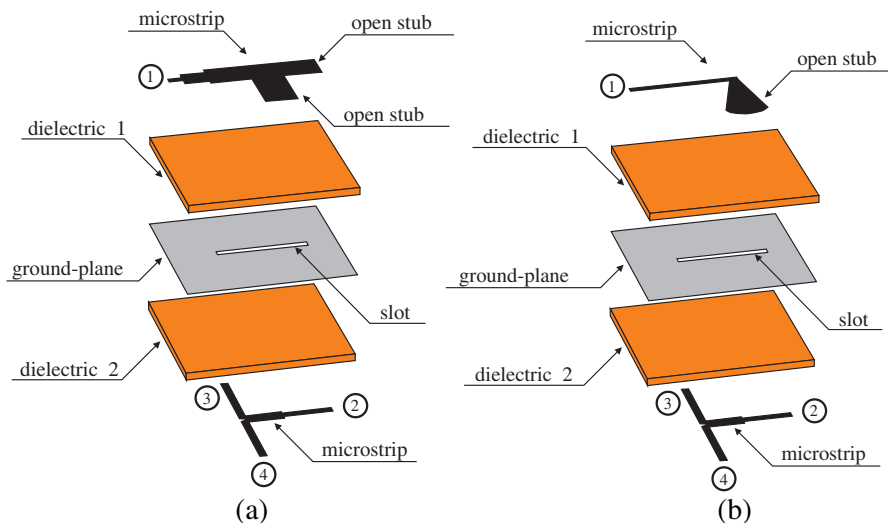


Figure 1. General view of the proposed structures of the magic-Ts: (a) With the rectangular open stub, (b) with the radial open stub.

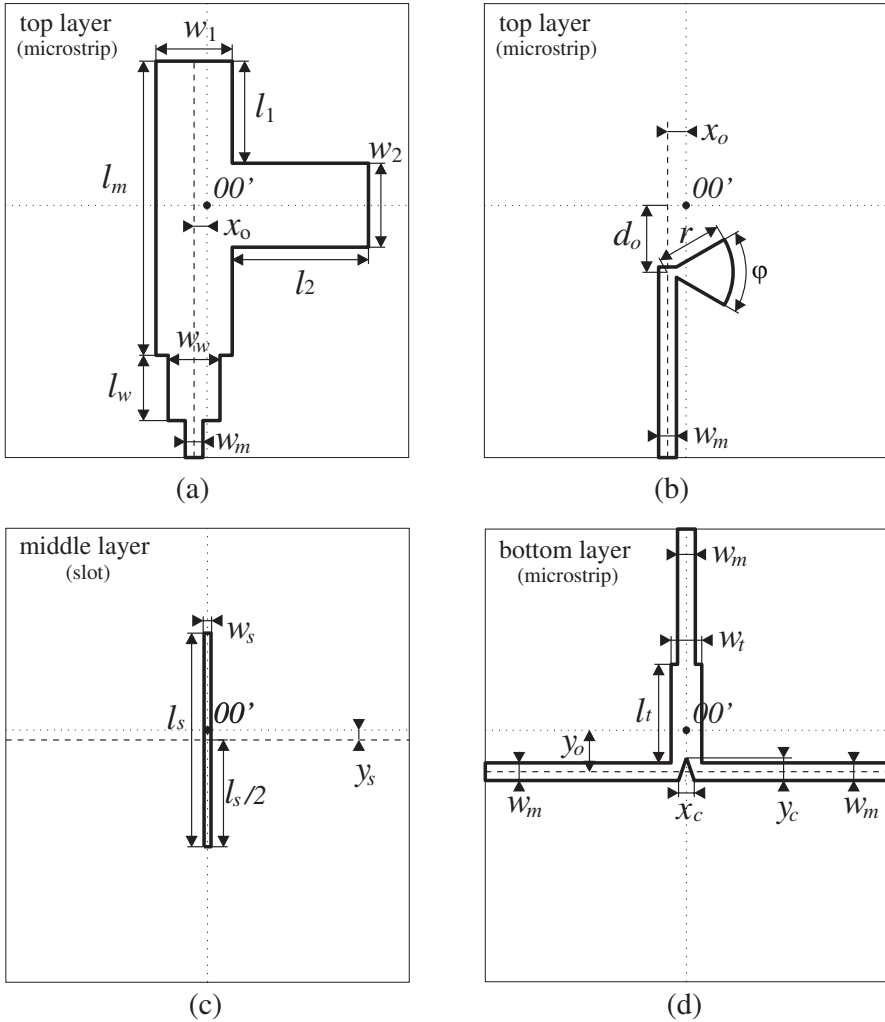


Figure 2. The structures of the magic-Ts: (a) Top layer of magic-T^A, (b) top layer of magic-T^B, (c) middle layer of magic-T^A and T^B, (d) bottom layer of magic-T^A and T^B.

slot arranged perpendicular to each other was used. In our solution we applied novel transitions in which the slot is coupled with a microstrip circuit and these elements are parallel. The circuits of both magic-Ts are presented in Fig. 2. The first arrangement, called T^A (see Fig. 2(a)), consists of two open circuited microstrip stubs attached to the microstrip arm which is matched using a quarter wave transformer.

In the second structure, signed T^B (see Fig. 2(b)), the radial stub is shunt-connected at the end of the open circuited microstrip arm. Both of these circuits are fed through port 1 corresponding to the difference port of the magic-T. The tee-junction circuit is placed on the opposite side of the structure and matched to port 2 by the quarter wave transformer (see Fig. 1).

2.2. Equivalent Circuits for the Considered Magic-Ts

The operation characteristics of the considered magic-Ts can be easily determined using their equivalent transmission line circuit models

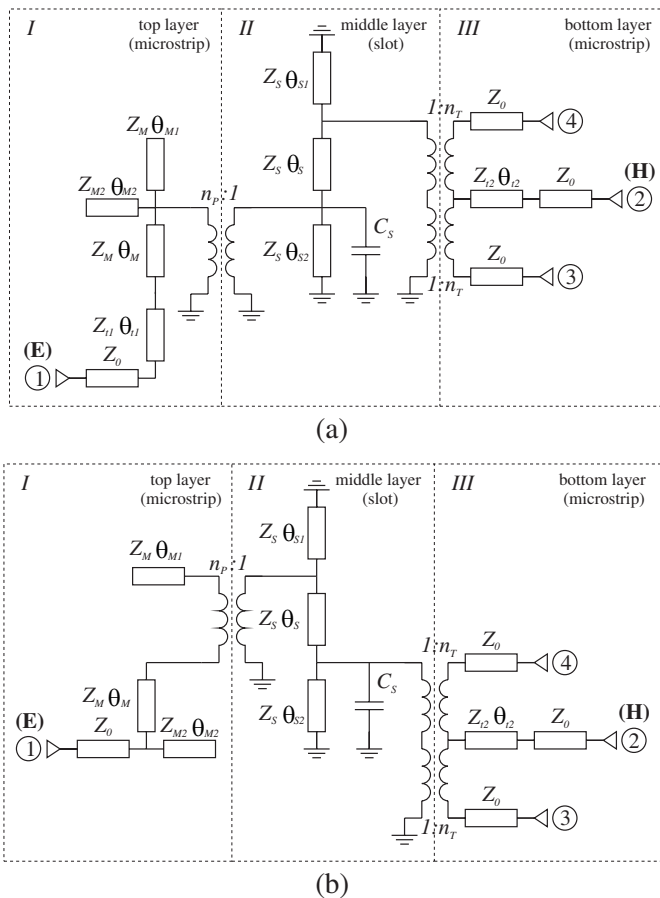


Figure 3. Circuit models of the proposed magic-T structures: (a) Magic-T^A, (b) magic-T^B.

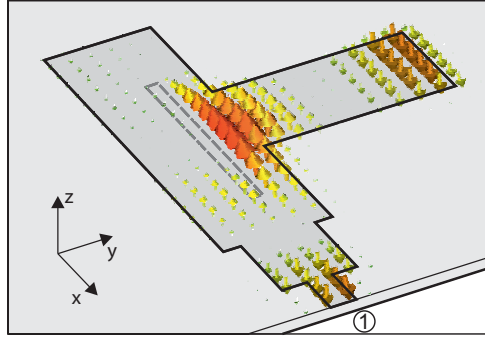


Figure 4. Electric field distribution between ground plane with slot and microstrip patch when port 1 is excited.

Table 1. Circuit and structure parameters of both magic-Ts.

magic-T ^A			
layer	circuit dimensions	structural parameters	equivalent circuit parameters
top	$w_1 = 7.56$ mm, $l_1 = 10.12$ mm, $w_2 = 8.32$ mm, $l_2 = 13.50$ mm, $w_w = 5.14$ mm, $l_w = 6.46$ mm, $w_m = 1.76$ mm, $l_m = 29.16$ mm, $x_o = 1.28$ mm,	$Z_M = 16.7 \Omega$, $\theta_M = 159^\circ$, $\theta_{M1} = 153^\circ$, $Z_{M2} = 15.4 \Omega$, $\theta_{M2} = 172^\circ$, $Z_0 = 50 \Omega$, $Z_{t1} = 22.8 \Omega$, $\theta_{t1} = 68^\circ$,	$Z_M = 16.7 \Omega$, $\theta_M = 180^\circ$, $\theta_{M1} = 123^\circ$, $Z_{M2} = 15.4 \Omega$, $\theta_{M2} = 209^\circ$, $Z_0 = 50 \Omega$, $Z_{t1} = 22.8 \Omega$, $\theta_{t1} = 90^\circ$, $n_P = 0.91$,
middle	$w_s = 0.82$ mm, $l_s = 17.03$ mm, $y_s = 0$ mm,	$Z_S = 48.6 \Omega$, $\theta_S = 42^\circ$, $\theta_{S1} = 45^\circ$, $\theta_{S2} = 87^\circ$	$Z_S = 80.9 \Omega$, $\theta_S = 4^\circ$, $\theta_{S1} = 71^\circ$, $\theta_{S2} = 75^\circ$, $C_S = 3.34$ pF,
bottom	$w_t = 3.05$ mm, $l_t = 9.79$ mm, $x_c = 1.58$ mm, $y_c = 2.25$ mm, $w_m = 1.76$ mm, $y_o = 4.13$ mm,	$Z_{t2} = 33.6 \Omega$, $\theta_{t2} = 101^\circ$, $Z_0 = 50 \Omega$,	$Z_{t2} = 35.4 \Omega$, $\theta_{t2} = 90^\circ$, $Z_0 = 50 \Omega$, $n_T = 0.53$,

magic-T ^B			
layer	circuit dimensions	structural parameters	equivalent circuit parameters
top	$d_o = 6.63 \text{ mm},$ $x_o = 1.84 \text{ mm},$ $w_m = 1.76 \text{ mm},$ $r = 6.5 \text{ mm},$ $\varphi = 60^\circ,$	$Z_M = 50 \Omega,$ $\theta_M = 18^\circ,$ $\theta_{M1} = 84^\circ,$ $\theta_{M2} = 9^\circ,$ $Z_0 = 50 \Omega,$	$Z_M = 50 \Omega,$ $\theta_M = 14^\circ,$ $\theta_{M1} = 60^\circ,$ $\theta_{M2} = 10^\circ,$ $Z_0 = 50 \Omega,$ $n_P = 0.54,$
middle	$w_s = 0.68 \text{ mm},$ $l_s = 21.17 \text{ mm},$ $y_s = 0.99 \text{ mm},$	$Z_S = 73.9 \Omega,$ $\theta_S = 63^\circ,$ $\theta_{S1} = 37^\circ,$ $\theta_{S2} = 100^\circ,$	$Z_S = 85.8 \Omega,$ $\theta_S = 7^\circ,$ $\theta_{S1} = 96^\circ,$ $\theta_{S2} = 103^\circ,$ $C_S = 0.003 \text{ pF},$
bottom	$w_t = 3.05 \text{ mm},$ $l_t = 9.79 \text{ mm},$ $x_c = 1.58 \text{ mm},$ $y_c = 2.25 \text{ mm},$ $w_m = 1.76 \text{ mm},$ $y_o = 0 \text{ mm},$	$Z_{t2} = 33.6 \Omega,$ $\theta_{t2} = 101^\circ,$ $Z_0 = 50 \Omega,$	$Z_{t2} = 35.4 \Omega,$ $\theta_{t2} = 90^\circ,$ $Z_0 = 50 \Omega,$ $n_T = 0.69,$

illustrated in Fig. 3. They consist of three circuits corresponding to the magic-T arrangements. Parameters Z_0 , Z_S , Z_t , Z_M stand for characteristic impedances of the ports, slotline, microstrip quarter wave transformers and other microstrip line sections, respectively. The lengths of the microstrip and slotline sections are defined by electrical lengths θ_M , θ_t and θ_S , respectively. The capacity C_S represents the electric field scattered at the edge of the slot and is concentrated between the slot area and strip of the patch. The appropriate impedance matching and mode conversion between the resonance slot (II) and resonance patch (I), as well as microstrip tee-junction (III), depend on the turn ratios n_P and n_T of the ideal transformers, respectively. The value of the turn ratio is approximately determined by $n = \sqrt{Z_M/Z_S}$. The required ratio of n_T of the impedance matching transformer between slot and tee-junction is used with the characteristic impedance of the dividing microstrip arms of the tee-junction. The turn ratio n_P between microstrip patch and slot in the magic-T^B circuit is calculated using characteristic impedance Z_M of the straight microstrip stub which is equivalent to the radial stub. As shown in [27], the radius of the radial stub is approximately equal to

$\lambda_m/6$, where λ_m is the wavelength of the equivalent straight microstrip stub determined by impedance Z_M and lengths θ_{M1} . The turn ratio n_P in the equivalent circuit of magic-T^A, shown in Fig. 3(a), is defined in a different way. Here, the broadband field conversion is controlled by the lengths of the open strip stubs for a fixed position of the slot in the junction. The modal TM_z electric field distribution plotted in Fig. 4 provides a conceptual understanding of the coupling between the junction and the slot. It can be seen that the excitation of the slot is similar as in the case of the transverse slot cut in the wall of the rectangular waveguide, which width is equal to a half of the wavelength in the microstrip arm of the patch. Hence, the required coupling ratio n_P can be achieved by adjusting the characteristic impedances of the fundamental mode in such a virtual waveguide and of the slot. The length of the resonance slot etched in the ground plane is approximately equal to $\lambda_s/2$ (where λ_s is the wavelength of the slotline) and it mainly determines centre operation frequency. The slot impedance is higher than the impedance of the microstrip arm. Therefore, a proper distance between the transverse symmetry plane of the slot and the radial stub, as well as tee-junction, allows obtaining appropriate coupling and matching conditions to ensure correct operation of the hybrid. To take into account the offset between the planes where the slot resonator is coupled with tee-junction and microstrip patch, the slot resonator is represented in the equivalent circuit model by the sections of transmission line Z_S with electrical lengths θ_S , θ_{S1} and θ_{S2} (see Fig. 3).

2.3. Structural and Equivalent Circuit Parameters of the Magic-T Structures

All magic-T configurations were optimized using the ADS Momentum. In the design an RF duroid substrate with the dielectric constant $\varepsilon_r = 3.5$, tangent losses $\tan \delta = 0.0018$ and thickness $h = 0.762$ mm is used. Both magic-T structures (T^A and T^B) were optimized to establish the optimum lengths of the slot and radial or straight stubs in the frequency range 4–6 GHz. The EM simulations have provided the dimensions of their circuits that are listed in Table 1 and they allowed for the definition of the corresponding structural parameters. Their characteristic impedances and electrical lengths were calculated analytically [28]. Additionally, Table 1 includes the circuit parameters resulting from the optimization of the magic-T equivalent circuits illustrated in Fig. 3. The objective function used in the optimization process was defined by the EM simulated transmission and reflection scattered coefficients of the investigated magic-T configurations.

The EM simulation accounts for field scattering effects, therefore,

the differences between the values of some structural and equivalent circuit parameters presented in Table 1, are observed. For example, the existence of the metallic strips located over the slot decreases the value of the slot characteristic impedance. For magic- T^A , the value of slot characteristic impedance $Z_S = 48 \Omega$ is smaller than its equivalent circuit value $Z_S = 80.9 \Omega$. In the equivalent circuit this effect is taken into account by capacitance which equals $C_S = 3.3 \text{ pF}$. Note, that in the magic- T^B structure the surface of the strip over the slot is much smaller than in the configuration of magic- T^A . This means that the slot parameters are less disturbed by the patch strips in magic- T^B . Actually, the characteristic impedances of the slot in the structural and equivalent circuits are similar and equal $Z_S = 73.9 \Omega$ and $Z_S = 85.8 \Omega$, respectively. In comparison to the capacitance C_S used in the magic- T^A circuit, its value is much smaller and equals 0.003 pF .

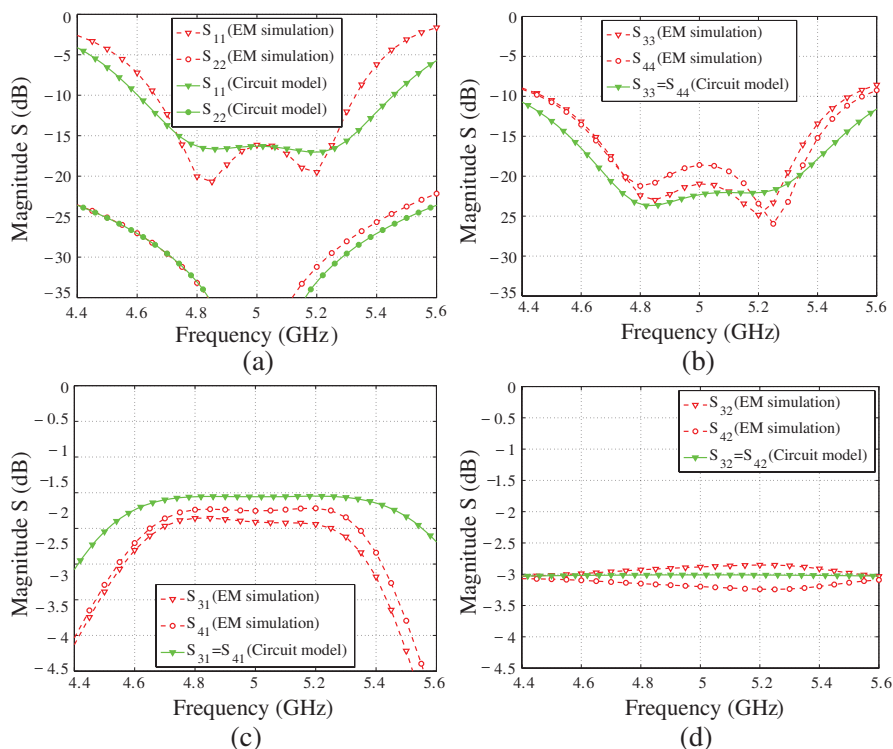


Figure 5. Simulated scattering parameters of magic- T^A : (a) Return losses at port 1 and 2, (b) return losses at port 3 and 4, (c) out-of-phase transmission, (d) in-phase transmission.

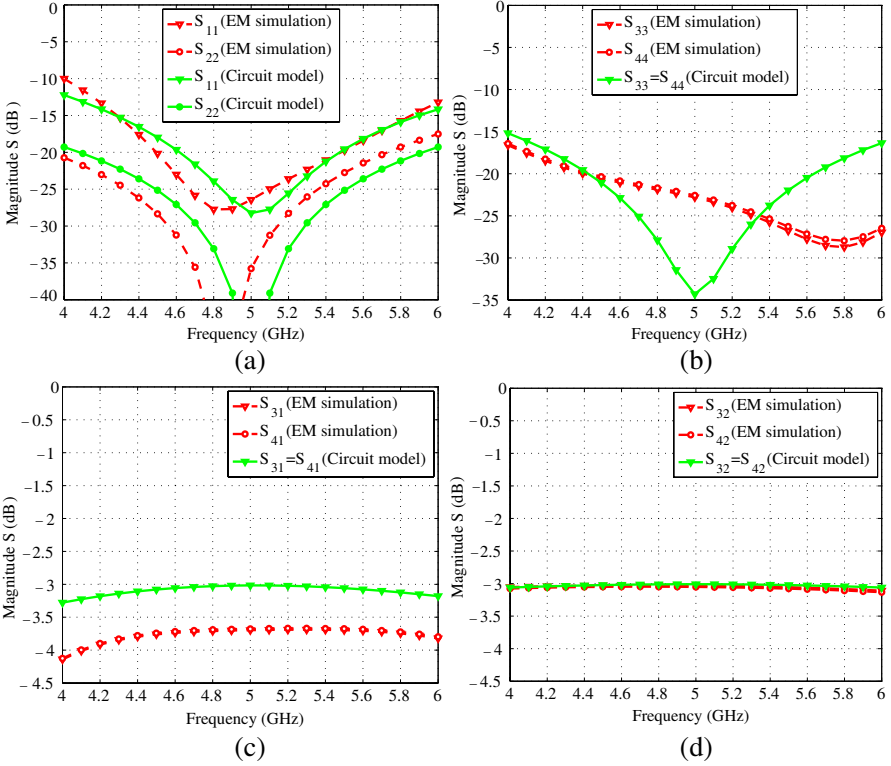


Figure 6. Simulated scattering parameters of magic- T^B : (a) Return losses at port 1 and 2, (b) return losses at port 3 and 4, (c) out-of-phase transmission, (d) in-phase transmission.

The scattering characteristics of the structures of magic- T^A and T^B , and their equivalent circuits are simulated using the ADS Momentum and Schematic Simulator (illustrated in Figs. 5 and 6, respectively). Note, that the results received from the simulations of such magic- T circuits are in good agreement with the ones obtained from their electromagnetic analyses. The discrepancies between the magnitudes of the signals in the dividing ports are smaller when both configurations are excited in the sum port. This is due to a better description of the tee-junction behaviour by its equivalent circuit than in the case of the slot-microstrip transition. Therefore, the magic- T performance is mainly affected by the construction of the microstrip-slotline transition. Due to the asymmetry of the microstrip patch in magic- T^A , the signals with different magnitudes appear at the dividing ports 3 and 4 for out-of-phase excitation. This asymmetrical effect is

Table 2. Comparison of the simulation results for several magic-T structures. The operation bandwidth determined for reflection losses at all ports better than 10 dB.

	double sided				two layer			
	Ref. [14]	Ref. [15]	Ref. [17]	Ref. [18]	Ref. [20]	Ref. [21]	magic -T ^A	magic -T ^B
center frequency (GHz)	2.0	2.35	10.0	6.7	7.0	5.45	5.0	5.0
fractional bandwidth (%)	50	71	29	71	43	40	16	40
insertion losses (dB)	4.0	4.3	4.0	5.0	3.8	4.0	4.7	3.9
amplitude imbalance (dB)	±0.2	±0.2	±0.3	±0.3	±0.2	±0.3	±0.2	±0.2
phase imbalance (deg)	±2.5	-	±1.6	±0.5	±1.4	±2.0	±2.0	±1.0
port 3-4 isolation (dB)	23	16	13	13	20	17	15	15
port E-H isolation (dB)	35	30	32	45	30	33	30	35

not taken into consideration by the equivalent circuit. For magic-T^A, the insertion losses S_{31} and S_{41} presented in Fig. 5 are less than 3.8 dB, while S_{32} and S_{42} are less than 3.5 dB in the frequency range from 4.7 to 5.3 GHz. As shown in Fig. 6, these magnitudes tend to be better for magic-T^B in a wider frequency range from 4 to 6 GHz. In the determined frequency bands the reflection coefficients in difference ports (1) are less than 15 dB.

The comparisons of EM simulated results for different types of magic-T arrangements are shown in Table 2. The presented parameters are defined at 10 dB reflection losses calculated at the difference port of the hybrid. From the proposed two-layer magic-T structures only the magic-T^B arrangement has broadband transmission characteristics similar to the previously reported hybrids realized in two-layer technology.

3. MEASURED RESULTS AND DISCUSSION

The prototypes of both magic-T configurations were fabricated and measured. The photographs of realized devices are shown in Fig. 7. The arrangements were measured using a vector network analyzer with SOLT calibration. The results were compared with the ones obtained from the ADS Momentum. The performance of magic-T^A is reported in Fig. 8. Both simulated and measured results reveal that within the frequency range from 4.6 to 5.4 GHz the insertion losses $S_{31(41)}$ for out-of-phase and $S_{32(42)}$ for in-phase excitation are less than 4.5 ± 0.2 dB and 3.8 ± 0.2 dB, respectively, while the return losses for ports 1 and 2 are better than 10 dB and 16 dB, respectively. The isolations S_{43} and S_{21} are greater than 15 dB and 30 dB, respectively. The frequency discrepancies between simulated and measured results and large insertion losses come probably in part from the inaccurate fabrication of the circuit and mismatch in the coaxial to microstrip transitions. As shown by the simulation, the inaccurate positioning of the slot and microstrip circuits affects the transmission between the narrow slotline and microstrip circuits. Further, it deteriorates the return losses S_{22} and isolation S_{21} which in effect reduces the bandwidth significantly. The measured and simulated results plotted in Fig. 9 again show the better performance and feasibility of the magic-T^B configuration. Although the measured data include the influence

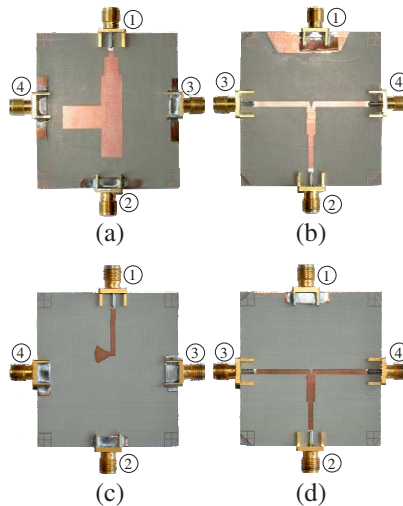


Figure 7. Photographs of the fabricated devices: (a) Top and (b) bottom of magic-T^A, (c) top and (d) bottom of magic-T^B.

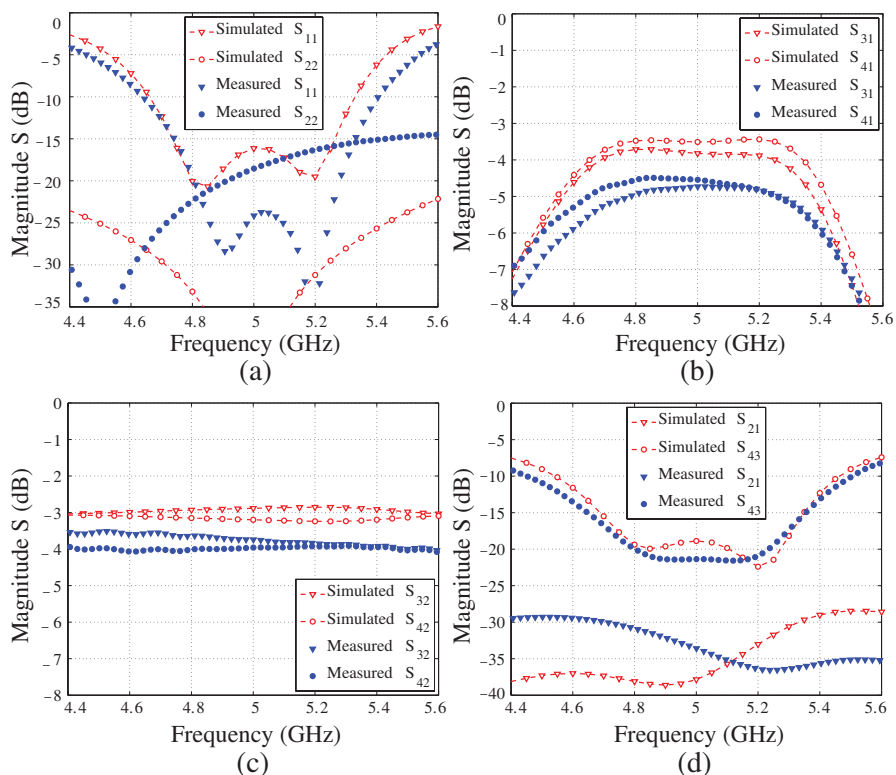
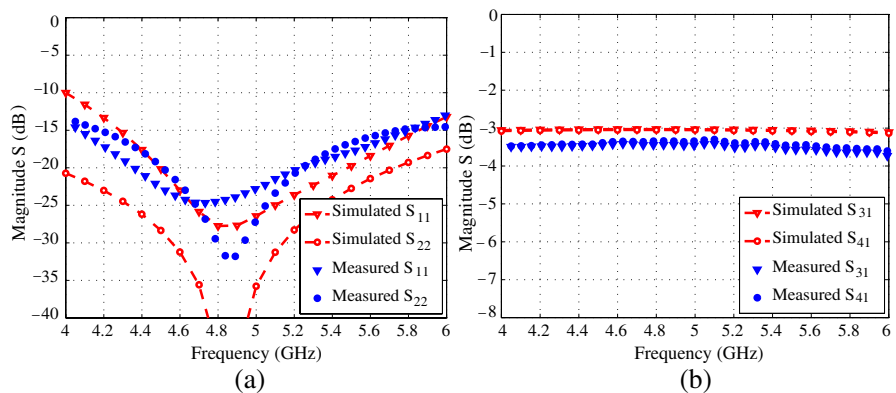


Figure 8. Simulated (EM) and measured scattering parameters of magic- T^A : (a) Return losses at port 1 and 2, (b) out-of-phase transmission, (c) in-phase transmission, (d) isolation.



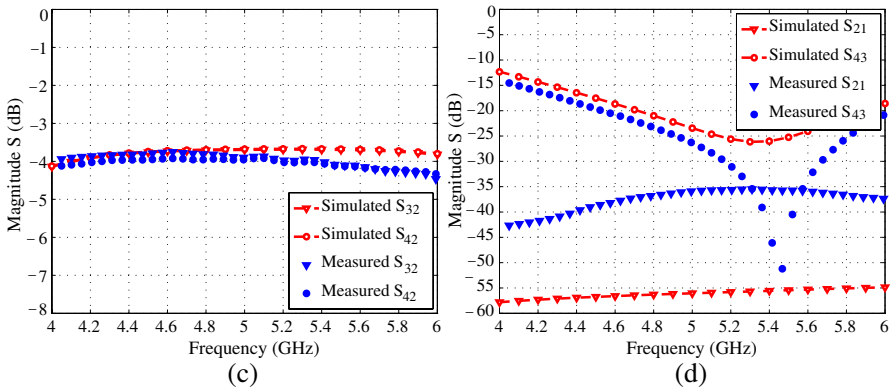


Figure 9. Simulated (EM) and measured scattering parameters of magic- T^B : (a) Return losses at port 1 and 2, (b) out-of-phase transmission, (c) in-phase transmission, (d) isolation.

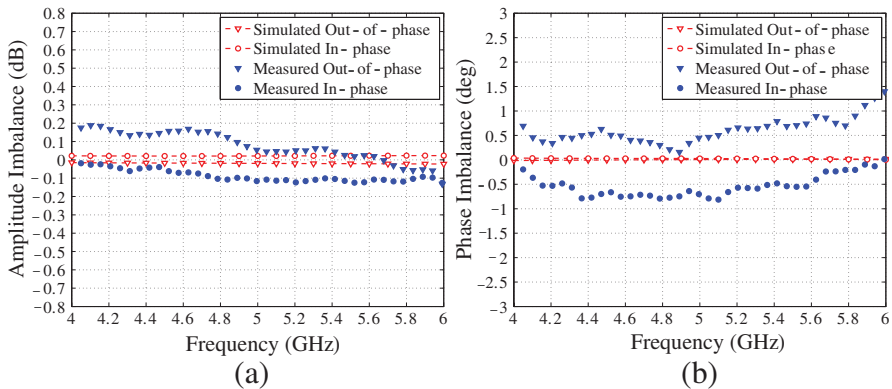


Figure 10. Simulated (EM) and measured results of magic- T^B : (a) Amplitude imbalance, (b) phase imbalance.

of the connectors, a good agreement with the simulation results is observed. The magic- T^B operates in the fractional bandwidth 40% within 4–6 GHz with return losses S_{11} and S_{22} better than 15 dB. The measured isolation S_{43} is greater than 15 dB, while S_{12} reaches magnitude better than 35 dB. For out-of-phase and in-phase excitation, the measured insertion losses $S_{31(41)}$ are equal to 4.0 ± 0.2 dB and $S_{32(42)}$ are less than 3.4 ± 0.2 dB, respectively. As shown in Fig. 10 the amplitude and phase imbalances for out-of-phase and in-phase are less than 0.2 dB and 1° , respectively.

4. CONCLUSION

Compact two-layer magic-Ts designed with novel microstrip-slotline transitions have been presented. The transitions utilize broadside coupling through the slot between microstrip patch and tee-junction printed at the top and bottom layers. In the proposed design the microstrip patch circuit and slotline are parallel to each other in comparison to the conventional perpendicular orientation commonly used in transitions. Both magic-Ts are analysed and designed utilizing equivalent circuit model and EM simulations. The first configuration uses a patch consisting of two open ended rectangular stubs. The simulation and measurement results indicate the narrow operation band of this configuration. Results have shown that this prototype has higher than 4 dB insertion losses in the frequency range 4.6–5.4 GHz. Good performance related to the insertion losses, isolation and balance were observed for the second magic-T configuration. For this structure the microstrip circuit of transition is modified and realized as a microstrip line folded at the end and terminated with radial resonator. This configuration shows good balance in the signal division together with small insertion losses for out-of-phase and in-phase operation across the frequency range 4–6 GHz. The phase deviation is below 1° over the operation bandwidth. Although the symmetry of the proposed magic-T configurations is slightly perturbed both considered structures exhibit isolation between their difference and sum ports better than 30 dB. Good agreement between the measured and predicted performance achieved for both developed configurations justify the analysis presented in this paper.

ACKNOWLEDGMENT

This work was supported by the Polish Ministry of Science and Higher Education in part from sources for science in the years 2012–2013 under Contract No. 0340/IP2/2011/71, from sources for science in the years 2010–2012 under COST Action IC0803, decision No. 618/N-COST/09/2010/0 and under funding for Statutory Activities for ETI Gdansk University of Technology.

REFERENCES

1. Wei, F., L. Chen, X.-W. Shi, Q.-Y. Wu, and Q.-L. Huang, "Design of compact UWB power divider with one narrow notch-band," *Journal of Electromagnetic Waves and Applications*, Vol. 24, Nos. 17–18, 2343–2352, 2010.

2. Kazerooni, M. and M. Aghalari, "Size reduction and harmonic suppression of rat-race hybrid coupler using defected microstrip structure," *Progress In Electromagnetics Research Letters*, Vol. 26, 87–96, 2011.
3. Qaroot, A. M., N. I. Dib, and A. A. Gheethan, "Design methodology of multi-frequency unequal split Wilkinson power dividers using transmission line transformers," *Progress In Electromagnetics Research B*, Vol. 22, 1–21, 2010.
4. Chiang, C. T. and B.-K. Chung, "Ultra wideband power divider using tapered line," *Progress In Electromagnetics Research*, Vol. 106, 61–73, 2010.
5. Kuo, J.-T. and C.-H. Tsai, "Generalized synthesis of rat race ring coupler and its application to circuit miniaturization," *Progress In Electromagnetics Research*, Vol. 108, 51–64, 2010.
6. Zhang, H., X.-W. Shi, F. Wei, and L. Xu, "Compact wideband gysel power divider with arbitrary power division based on patch type structure," *Progress In Electromagnetics Research*, Vol. 119, 395–406, 2011.
7. Deng, P.-H., J.-H. Guo, and W.-C. Kuo, "New Wilkinson power dividers based on compact stepped-impedance transmission lines and shunt open stubs," *Progress In Electromagnetics Research*, Vol. 123, 407–426, 2012.
8. Sedighy, S. H. and M. Khalaj-Amirhosseini, "Compact Wilkinson power divider using stepped impedance transmission lines," *Journal of Electromagnetic Waves and Applications*, Vol. 25, No. 13, 1773–1782, 2011.
9. Liu, G.-Q., L.-S. Wu, and W.-Y. Yin, "A compact microstrip rat race coupler with modified lange and t-shaped arms," *Progress In Electromagnetics Research*, Vol. 115, 509–523, 2011.
10. Li, Q., X.-W. Shi, F. Wei, and J. G. Gong, "A novel planar 180° out-of-phase power divider for UWB application," *Journal of Electromagnetic Waves and Applications*, Vol. 25, No. 1, 161–167, 2011.
11. Howe, H., *Stripline Circuit Design*, Artech House, Norwood, MA., 1974.
12. Ho, C.-H., L. Fan, and K. Chang, "New uniplanar coplanar waveguide hybrid-ring couplers and magic-ts," *IEEE Transactions on Microwave Theory and Techniques*, Vol. 42, No. 12, 2440–2448, December 1994.
13. Aikawa, M. and H. Ogawa, "A new MIC magic-T using coupled slot lines," *IEEE Transactions on Microwave Theory and*

- Techniques*, Vol. 28, No. 6, 523–528, June 1980.
14. Kim, J. P. and W. S. Park, “Novel configurations of planar multilayer magic-T using microstrip-slotline transitions,” *IEEE Transactions on Microwave Theory and Techniques*, Vol. 50, No. 7, 1683–1688, July 2002.
 15. Cheng, C. H. and Q. Gao, “A novel broadband magic-T using microstrip-slotline transitions,” *Microwave and Optical Technology Letters*, Vol. 46, No. 6, 585–588, September 2005.
 16. Yu, Y. W., G. M. Wang, and Y. Ding, “A novel wideband planar magic-T,” *International Conference on Microwave and Millimeter Wave Technology, ICMMT*, Vol. 1, 315–317, 2008.
 17. Kongpop, U., E. J. Wollack, S. H. Moseley, J. Papapolymerou, and J. Laskar, “A compact low-loss magic-T using microstrip-slotline transitions,” *IEEE/MTTS International Microwave Symposium*, 37–40, June 2007.
 18. Bialkowski, M. E. and Y. Wang, “Design of UWB uniplanar 180° hybrid employing ground slots and microstrip-slot transitions,” *18th International Conference on Microwave Radar and Wireless Communications (MIKON)*, 1–4, June 2010.
 19. Abbosh, A. M. and M. E. Bialkowski, “Design of a UWB planar 180° hybrid exploiting microstrip-slot transitions,” *Microwave and Optical Technology Letters*, Vol. 49, No. 6, 1343–1346, June 2007.
 20. Feng, W., Q. Xue, and W. Che, “Compact planar magic-T based on the double-sided parallel-strip line and the slotline coupling,” *IEEE Transactions on Microwave Theory and Techniques*, Vol. 58, No. 11, 2915–2923, November 2010.
 21. Davidovitz, M., “A compact planar magic-T junction with aperture-coupled difference port,” *IEEE Microwave and Guided Wave Letters*, Vol. 7, No. 8, 217–218, August 1997.
 22. He, F. F., K. Wu, W. Hong, H. J. Tang, H. B. Zhu, and J. X. Chen, “A planar magic-T using substrate integrated circuits concept,” *IEEE Microwave and Wireless Components Letters*, Vol. 18, No. 6, 386–388, June 2008.
 23. Liu, M. and Z. Feng, “A novel hybrid planar SIW magic tee and monopulse antenna,” *Microwave and Optical Technology Letters*, Vol. 52, No. 3, 686–689, March 2010.
 24. Feng, W., W. Che, and K. Deng, “Compact planar magic-T using E-plane substrate integrated waveguide (SIW) power divider and slotline transition,” *IEEE Microwave and Wireless Components Letters*, Vol. 20, No. 6, 331–333, June 2010.
 25. Liu, B., W. Hong, Y.-Q. Wang, Q.-H. Lai, and K. Wu, “Half mode

- substrate integrated waveguide (HMSIW) 3-dB coupler,” *IEEE Microwave and Wireless Components Letters*, Vol. 17, No. 1, 22–24, January 2007.
26. Schiek, B. and J. Kohler, “An improved microstrip-to-microslot transition (letters),” *IEEE Transactions on Microwave Theory and Techniques*, Vol. 24, No. 4, 231–233, April 1976.
 27. Zinieris, M. M., R. Sloan, and L. E. Davis, “A broadband microstrip-to-slot-line transition,” *Microwave and Optical Technology Letters*, Vol. 18, No. 5, 339–342, August 1998.
 28. Marynowski, W., P. Kowalczyk, and J. Mazur, “On the characteristic impedance definition in microstrip and coplanar lines,” *Progress In Electromagnetics Research*, Vol. 110, 219–235, 2010.